JVSTB Journal of Vacuum Science & Technology B

Molecular-beam-epitaxy growth of high-quality In Ga As N Ga As quantum well lasers emitting at 1.3 m

J. S. Wang, R. S. Hsiao, G. Lin, K. F. Lin, H. Y. Liu, C. M. Lai, L. Wei, C. Y. Liang, J. Y. Chi, A. R. Kovsh, N. A. Maleev, D. A. Livshits, J. F. Chen, H. C. Yu, and V. M. Ustinov

Citation: Journal of Vacuum Science & Technology B **22**, 2663 (2004); doi: 10.1116/1.1807839
View online: http://dx.doi.org/10.1116/1.1807839
View Table of Contents: http://scitation.aip.org/content/avs/journal/jvstb/22/6?ver=pdfcov
Published by the AVS: Science & Technology of Materials, Interfaces, and Processing

Molecular-beam-epitaxy growth of high-quality InGaAsN/GaAs quantum well lasers emitting at 1.3 μm

J. S. Wang[a)]
Industrial Technology Research Institute (OES/ITRI), 310 Hsinchu, Taiwan, Republic of China and Department of Physics, Chung Yuan Christian University, Chung-Li (32023), Taiwan, Republic of China

R. S. Hsiao
Industrial Technology Research Institute (OES/ITRI), 310 Hsinchu, Taiwan, Republic of China and Department of Electrophysics, National Chiao Tung University, 310 Hsinchu, Taiwan, Republic of China

G. Lin, K. F. Lin, H. Y. Liu, C. M. Lai, L. Wei, C. Y. Liang, and J. Y. Chi
Industrial Technology Research Institute (OES/ITRI), 310 Hsinchu, Taiwan, Republic of China

A. R. Kovsh, N. A. Maleev, and D. A. Livshits
Industrial Technology Research Institute (OES/ITRI), 310 Hsinchu, Taiwan, Republic of China and A. F. Ioffe Physico-Technical Institute, 194021, St. Petersburg, Russia

J. F. Chen
Department of Electrophysics, National Chiao Tung University, 310 Hsinchu, Taiwan, Republic of China

H. C. Yu
Industrial Technology Research Institute (OES/ITRI), 310 Hsinchu, Taiwan, Republic of China and Institute of Microelectronics, National Cheng Kung University, 701 Tainan, Taiwan, Republic of China

V. M. Ustinov
A. F. Ioffe Physico-Technical Institute, 194021, St. Petersburg, Russia

(Received 16 April 2004; accepted 23 August 2004; published 5 November 2004)

Molecular-beam-epitaxy growth of high structural and optical-quality InGaAsN/GaAs quantum wells (QW) has been investigated. The material quality can be improved significantly by using low-temperature growth to suppress the phase separation. High-performance ridge-waveguide InGaAsN/GaAs single QW lasers emitting at 1.3 μm have been demonstrated. Infinite-cavity-length threshold-current density of 400 A/cm^2, internal quantum efficiency of 96%, and a slope efficiency of 0.67 W/A for a cavity length $L=1$ mm were obtained. A TO46 packaging laser shows single lateral-mode kink-free output power of more than 200 mW with a maximum total wallplug efficiency of 29% at room temperature under continuous wave (cw) operation. Moreover, 1.3 μm InGaAsN/GaAs QW vertical-cavity surface-emitting lasers with a threshold current density lower than 2 KA/cm^2 at room temperature have been achieved. We obtained multimode cw output power and slope efficiency in excess of 1 mW and 0.15 W/A, respectively. © *2004 American Vacuum Society.* [DOI: 10.1116/1.1807839]

I. INTRODUCTION

1.3 μm vertical-cavity surface-emitting lasers (VCSELs) are promising transmitter devices for short and midrange optical networks because these lasers can be used for standard single-mode and multimode silica fibers. The primary challenge in making a 1.3 μm VCSEL has been the integration of high-reflectivity distributed Bragg reflectors (DBRs) with a suitable active region. A single-mode VCSEL emitting more than 2 mW cw power near 1.3 μm has been presented by Jayaraman *et al.*[1] using a double wafer-fused structure consisting of an InP-based active region combined with AlGaAs DBR mirrors. Recently, progress in developing active regions that can be grown directly on a GaAs substrate has resulted in room-temperature cw operation of monolithically grown 1.3 μm VCSELs using either InGaAsN or GaAsSb quantum wells (QWs) or InAs quantum dots.[2–5] AlGaAs/GaAs Bragg mirrors have a high index contrast as well as good thermal conductivity. Temperature stability of InGaAsN lasers has been shown to be superior to that of InP based lasers,[6,7] but the absolute values of their threshold current densities are still high, due to crystal defects formed by the phase separation of nitrogen incorporation. This makes quantitative comparison difficult. In this article, we report our recent results in the development of an InGaAsN-based approach to long-wavelength GaAs lasers grown by molecular-beam epitaxy (MBE) under low growth temperatures. These temperatures can suppress nonradiative recombination defects formed during nitrogen incorporation. An infinite-cavity-length threshold-current density of 400 A/cm^2 was obtained for the 1.3-μm ridge-waveguide InGaAsN/GaAs single-quantum-well (SQW) edge-emitting lasers. The internal quantum efficiency of 96% and the slope efficiency of 0.67 W/A with a cavity length of $L=1$ mm were obtained. The cw kink-free output power of the single

[a)]Electronic mail: jswang@cycu.edu.tw

lateral-mode laser is more than 200 mW with a maximum total wallplug efficiency of 29%. Moreover, 1.3 μm VCSELs with a threshold current density lower than 2 KA/cm^2 at room temperature have been achieved. To the best of our knowledge, this is the lowest value ever reported for InGaAsN/GaAs QW VCSELs. Multimode cw output power and slope efficiency are higher than 1 mW and 0.15 W/A, respectively.

II. InGaAsN/GaAs SQW GROWTH

The structures were grown on n^+ type (100) GaAs substrates using a Riber Epineat solid-source MBE. An EPI-Unibulb radio-frequency (rf) plasma source was used to supply active nitrogen species from ultra-pure N_2 gas. The intensity of the plasma can be controlled by the rf power and the flow rate of N_2. A photodetector was employed to measure the plasma-light intensity based on the photodetector voltage V_{OPT}. A mechanical gate valve located between the growth chamber and plasma cell was used to control the irradiation of the nitrogen beam during the growth of InGaAsN QW layers. The indium and gallium were supplied from conventional Knudsen effusion cells. Arsenic in the form of As_4 was supplied from a cracker source. The low-growth temperature of around 420 °C measured by a pyrometer was used in InGaAs(N) SQWs to suppress the phase separation[8] while the growth temperature of GaAs layers was 600 °C. Two samples with 2.2% nitrogen content and without nitrogen content were grown while keeping the indium and gallium cell temperatures constant to give a 34% indium and 66% gallium composition. To remove the defects caused by low temperature growth, 10 min *in situ* 700 °C annealing was used after a GaAs cap layer was grown. The surface morphology during growth of InGaAsN QWs was monitored *in situ* by reflection high-energy electron diffraction. X-ray diffraction (XRD) was carried out with a Bede four/crystals/high-resolution x-ray diffractometer. The indium and nitrogen compositions of InGaAsN SQWs were determined by fitting the XRD spectra using commercial dynamic-simulation software (RADS). Photoluminescence (PL) data was obtained using an argon-ion laser and a THR 1000 spectrometer with an InGaAs photodetector.

Figure 1 shows the normalized XRD spectra of the InGaAs(N)/GaAs SQW samples. The solid curves are experimental results, while the dotted curves are the results of best curve fitting using RADS. The fitted indium composition was obtained from an InGaAs/GaAs SQW, and then the fitted nitrogen composition was obtained by assuming the indium composition was the same. As can be seen in Fig. 1, nitrogen incorporation shifts the XRD peak of the SQW toward the substrate peak, which indicates a reduction of the lattice mismatch. Note that the full width at half maximum (FWHM) of the SQW peak in the InGaAsN/GaAs sample is smaller than that of the InGaAs/GaAs sample. Furthermore, the fringe features from the GaAs caps in the InGaAsN/GaAs sample are clearer and have better fitting results than the InGaAs/GaAs sample. This shows that flatter

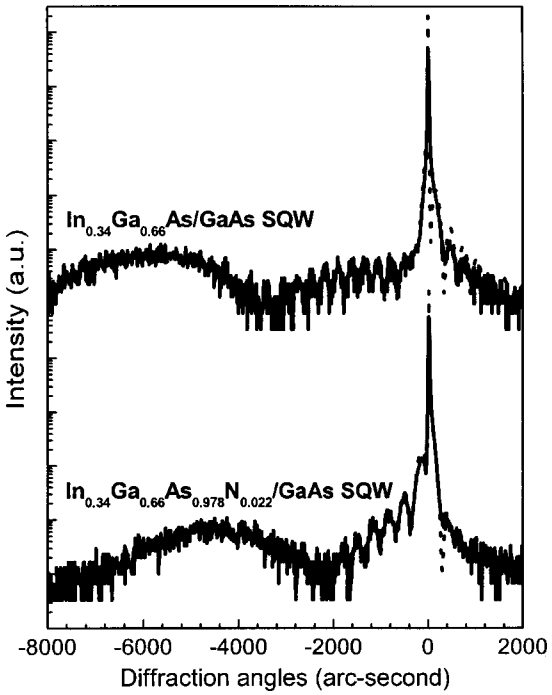

FIG. 1. X-ray diffraction spectra of InGaAs(N)/GaAs SQW samples. The solid curves are experimental results, while the dotted curves are the results of best curve fitting using the dynamic simulation software.

heterointerfaces are achieved in the InGaAsN/GaAs SQW samples due to their smaller lattice mismatch.

Figure 2 shows the room-temperature PL spectra of the InGaAs(N)/GaAs SQW samples. As can be seen, the PL peak wavelength shifts from 1.13 to 1.34 μm with nitrogen at a concentration of 2.2%. This result confirms a band-gap bowing effect due to the incorporation of nitrogen. Note that the integrated PL intensity is improved with nitrogen incor-

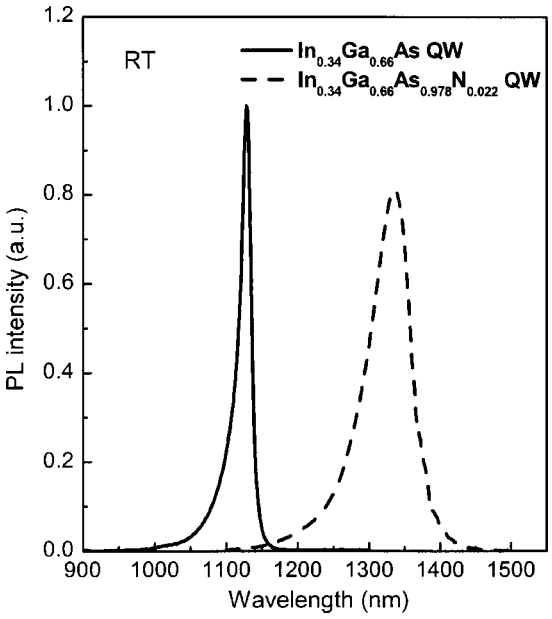

FIG. 2. Room-temperature PL spectra of InGaAs(N)/GaAs SQW samples.

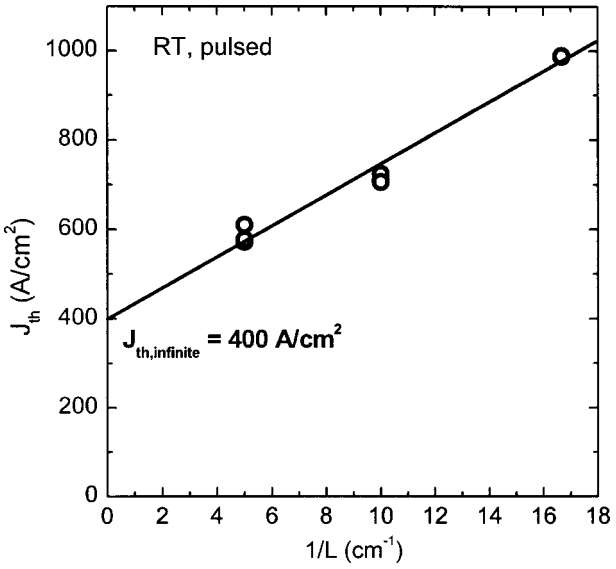

FIG. 3. Threshold current density versus reciprocal cavity length for 1.3 μm InGaAsN lasers.

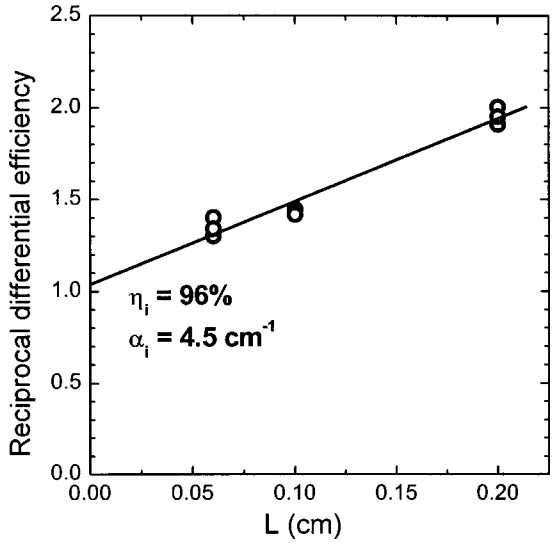

FIG. 4. Reciprocal differential efficiency vs cavity length for 1.3 μm InGaAsN lasers.

poration, which may be due to the reduction of defects caused by reducing the lattice mismatch. This indicates that the optical quality of InGaAsN QW can be improved significantly by using low-temperature growth to suppress the phase separation. However, the FWHM increases most likely due to the composition fluctuation of the InGaAsN alloy.

III. RIDGE-WAVEGUIDE SQW EDGE-EMITTING LASERS

The lasers consisted of a 1.6-μm-thick *n*-doped $Al_{0.3}Ga_{0.7}As$ cladding layer, a 6.5-nm-thick $In_{0.34}Ga_{0.66}As_{0.978}N_{0.022}$ SQW embedded in an undoped GaAs waveguide, a 1.6-μm-thick *p*-doped $Al_{0.3}Ga_{0.7}As$ cladding, and a p^+ GaAs contact layer. Growth temperature was 700 °C for the cladding layer and 420 °C for the InGaAsN QW layer, respectively. *In situ* annealing was done during the cladding-layer growth. A ridge waveguide of 3 μm width was fabricated by a double-channel ridge-waveguide self-aligned process. Ti/Pt/Au and Ni/Ge/Au were deposited for *p* and *n* contacts, respectively. The pulsed measurements were performed under a pulse width of 1 μs and a repetition rate of 10 KHz.

Figure 3 shows the threshold-current density versus the reciprocal cavity length for 1.3 μm InGaAsN/GaAs SQW lasers. The infinite-cavity-length threshold-current density is 400 A/cm^2. The dependence of the reciprocal differential efficiencies on the cavity length is shown in Fig. 4. As can be seen, an internal quantum efficiency of 96% with an internal loss of 4.5 cm^{-1} and a slope efficiency of 0.67 W/A for a cavity length of $L=1$ mm were achieved. Figure 5(a) shows cw operation of the ridge-waveguide laser diode after antireflection (AR)/high-reflection (HR) facet coating, bonding, and packaging in a TO46 can. The lasing spectrum shows in the inset. The far-field patterns under different injection current, as shown in Fig. 5(b), shows single-mode operation up to the highest power recorded. Threshold current and differential efficiency are 22 mA and 62%, respectively. The maximum value of 210 mW of single-mode output power is limited by thermal rollover. To the best of our knowledge,

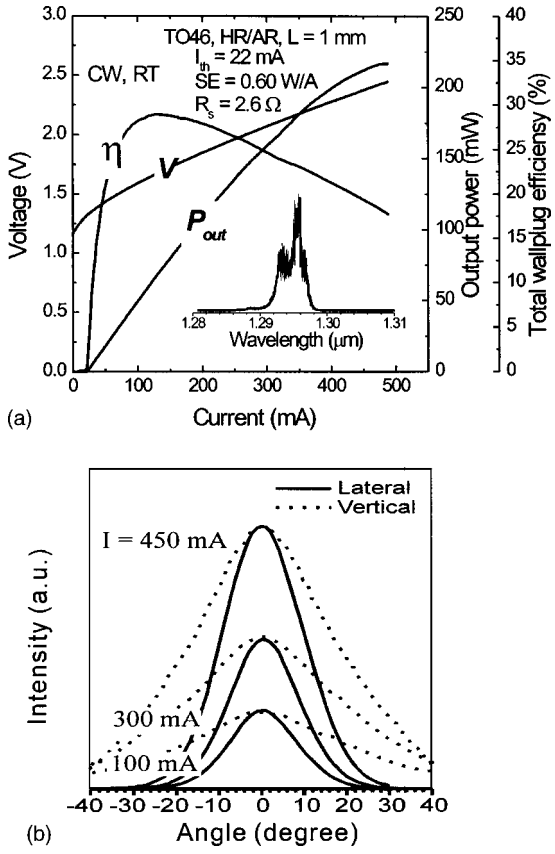

FIG. 5. (a) Output power and wallplug efficiency vs current under cw operation for a HR/AR coating 1-mm-long InGaAsN laser with TO46 package. The inset shows the lasing spectrum. (b) Far-field patterns under different injection current.

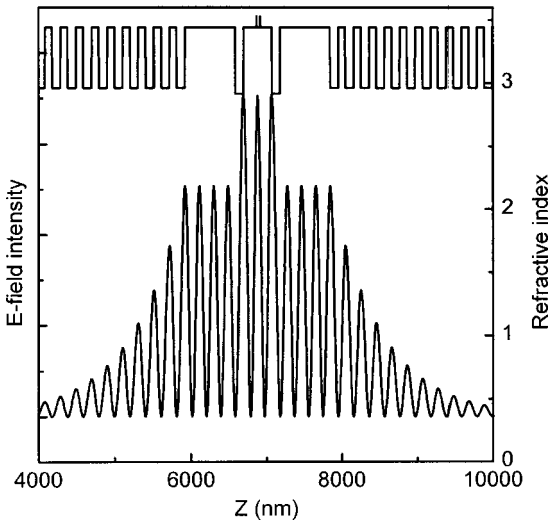

FIG. 6. Schematic of the E-field intensity and refractive index profile around the microcavity of intracavity-contacted VCSEL.

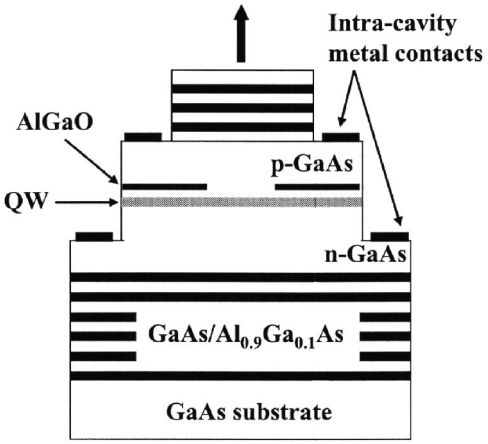

FIG. 7. Schematic of a fabricated intracavity-contacted VCSEL.

this is the highest value ever reported for single-mode 1.3-μm-range lasers based on GaAs substrates.

IV. VCSELs

The active region of the VCSEL structure consisted of two 6-nm-thick InGaAsN QWs containing 34% indium and 2% nitrogen, separated by a 12-nm-thick GaAs layer. Point defects formed during growth at such low temperatures were removed by annealing at 750 °C for 10 min after deposition of a 55-nm-thick $Al_{0.98}Ga_{0.02}As$ current-confinement aperture layer. To target high-frequency operation and avoid free-carrier absorption in *p*-doped materials, we chose an intracavity contacted configuration with undoped AlGaAs mirrors and a conventional (*p*-*i*-*n*) diode design inside the cavity. The schematic of the electric-field intensity and refractive-index profile around the microcavity is shown in Fig. 6. The total thickness of the cavity was 5λ (1888 nm). An undoped core GaAs layer of 1λ (377.6 nm) thickness contained the active region of two InGaAsN QWs. Beryllium and silicon were used as *p*- and *n*-type dopants, respectively. Three thin GaAs layers heavily doped with beryllium were located at the minima of the optical field to reduce serial resistance and improve current-spreading uniformity. The top and bottom mirrors consisted of 25 and 33 pairs of $Al_{0.9}Ga_{0.1}As/GaAs$ layers, respectively. After epitaxial growth, the VCSELs were fabricated into electrically injected intracavity contacted devices, as shown schematically in Fig. 7. A two-step mesa pattern with diameters of 20 and 60 μm, respectively, was defined on the wafer surface by using dry etching. Next, the $Al_{0.98}Ga_{0.02}As$ aperture layer was selectively oxidized at 420 °C. Finally, intracavity metal contacts were deposited by e-beam evaporation using a lift-off process.

Figure 8 shows light-current-voltage curves of a VCSEL with an 18 μm aperture. An oxide aperture diameter of 18 μm was determined by an optical microscope on the test devices without the top DBR prepared in the same oxidation run. The near-field pattern and optical spectrum of the devices driven at I_{th} are shown in the inset. The lasing wavelength was 1304 nm. Note that light disappears in the left corner of the pattern due to the misalignment of the *p*-metal contact. The threshold current is 4 mA and the corresponding voltage is 2.5 V. A computer simulation of the near-field pattern, taking into account the current-spreading nonuniformity, shows that lasing occurs at a threshold current density below 2 KA/cm^2. To the best of our knowledge, this is the lowest value ever reported for InGaAsN/GaAs QW VCSELs emitting at 1.3 μm. As can be seen in Fig. 8, the room-temperature output power is more than 10 mW with an initial slope efficiency of 0.20 W/A under pulsed operation. CW output power exceeds 1 mW with an initial slope efficiency of 0.15 W/A. In spite of the high quality of the active region, the device performance is limited by the thermal heating. We believe that significant improvement in VCSEL performance can be achieved with further optimization of the VCSEL structure design and processing procedure. The temperature dependence of the threshold current is shown in Fig. 9. The minimum threshold current is well below room temperature. This fact indicates nonoptimal detuning of the gain

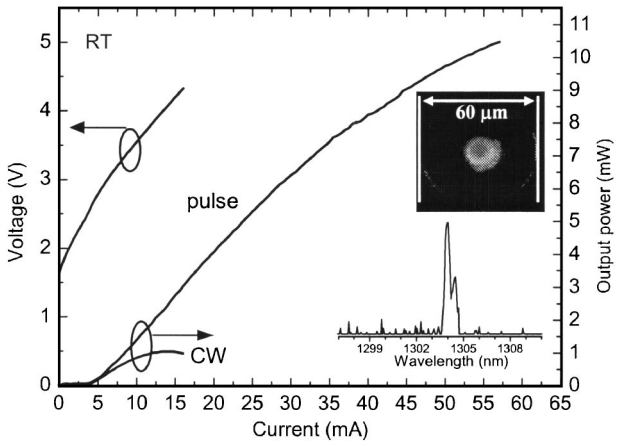

FIG. 8. Room-temperature light-current-voltage curves of 1.3 μm VCSELs with an 18 μm aperture. The inset shows the near-field pattern and optical spectrum of the devices driven at I_{th}.

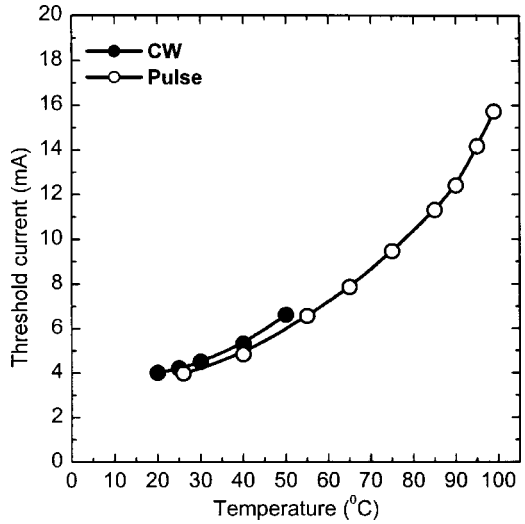

FIG. 9. Temperature dependence of threshold current of 1.3 μm VCSELs.

peak and cavity resonance. Thus, following optimization of the detuning of the gain peak and cavity resonance can result in a longer wavelength, higher maximum output power, and better over-temperature performance in future devices.

V. CONCLUSIONS

We have demonstrated the successful MBE growth of high-quality InGaAsN/GaAs SQW under low-growth-temperature conditions. An infinite-cavity-length threshold-current density of 400 A/cm^2 with internal quantum efficiency of 96% and a slope efficiency of 0.67 W/A for 1 mm cavity length have been obtained for a 1.3 μm ridge-waveguide InGaAsN/GaAs SQW edge-emitting laser, which indicates the high quality of the InGaAsN/GaAs active region. The RT-cw kink-free output power of a single lateral-mode laser is more than 200 mW with a maximum total wallplug efficiency of 29%. Moreover, 1.3 μm VCSELs with a threshold current density less than 2 KA/cm^2 reported for an InGaAsN/GaAs active region at room temperature under cw operation has been demonstrated. We have demonstrated multimode output power and slope efficiency in excess of 1 mW and 0.15 W/A, respectively.

ACKNOWLEDGMENTS

The authors gratefully acknowledge the technical assistance of C. Y. Huang and F. I. Lai. This work was funded by the ITRI-Ioffe Joint Scientific Program and National the Republic of China Program on Nanoscience and Nanotechnology.

[1]V. Jayaraman, M. Mehta, A. W. Jackson, S. Wu, Y. Okuno, J. Piprek, and J. E. Bowers, IEEE Photonics Technol. Lett. **15**, 1495 (2003).
[2]G. Steinle, H. Riechert, and A. Yu. Egorov, Electron. Lett. **37**, 93 (2001).
[3]A. Ramakrishnan, G. Steinle, D. Supper, C. Degen, and G. Ebbinghaus, Electron. Lett. **38**, 322 (2002).
[4]M. Yamada, T. Anan, K. Kurihara, K. Nishi, K. Tokutome, A. Kamei, and S. Sugou, Electron. Lett. **36**, 637 (2000).
[5]J. A. Lott, N. N. Ledentsov, V. M. Ustinov, N. A. Maleev, A. E. Zhukov, A. R. Kovsh, M. V. Maximov, B. V. Volovik, Zh. I. Alferov, and D. Bimberg, Electron. Lett. **36**, 1384 (2000).
[6]S. Illek, A. Ultsch, B. Borchert, A. Yu. Egorov, and H. Riechert, Electron. Lett. **36**, 725 (2000).
[7]B. Borchert, A. Yu. Egorov, S. Illeks, M. Komainda, and H. Riechert, Electron. Lett. **35**, 2204 (1999).
[8]J. S. Wang, A. R. Kovsh, R. S. Hsiao, L. P. Chen, J. F. Chen, T. S. Lay, and J. Y. Chi, J. Cryst. Growth **262**, 84 (2004).